Solar Wind Charge Exchange X-rays at Mars

H. Gunell* and M. Holmström†
Swedish Institute of Space Physics, Kiruna, Sweden

E. Kallio and P. Janhunen
Finnish Meteorological Institute, Box 503 FIN-00101 Helsinki, Finland

K. Dennerl
Max-Planck-Institut für extraterrestrische Physik, Garching, Germany

Abstract:
Wherever the solar wind meets a neutral atmosphere, X-rays are emitted by a charge exchange process between the neutrals and heavy solar wind ions.

A hybrid simulation of the solar wind-Mars interaction and a test particle simulation of heavy ion trajectories near Mars is used to compute the contribution from charge exchange processes to the X-ray emission from Mars. The results are compared to observations of X-rays from Mars made with the Chandra telescope [1]. The comparison indicates that the solar wind charge exchange process is a likely candidate for the production of the X-ray halo at Mars.

The calculations were performed in three steps. First the solar wind parameters were estimated. We compare the results of two different solar wind parameter estimates: A ballistic model based on data obtained by the WIND spacecraft, and an MHD model using input from interplanetary scintillation measurements. These two models produce X-ray images with significantly different structure. The intensity of the X-ray emissions and the size of the X-ray halo are also found to increase with an increasing exobase neutral temperature [2].

The second step was running a hybrid simulation of the interaction between the solar wind and Mars to obtain the electric and magnetic fields around Mars.

As a third step a test particle simulation was run, calculating the trajectories of heavy solar wind ions in the electric and magnetic fields that were obtained from the hybrid simulation. The X-ray emission density was saved on a grid for each time step of the test particle simulation. A hundred thousand trajectories were calculated for each of the ion species O^{7+}, C^{6+}, O^{6+}, O^{8+}, Mg^{10+}, Mg^{9+}, Si^{9+}, N^{6+}, C^{5+}, Ne^{8+}, Fe^{9+}, S^{9+}, Si^{8+}, Fe^{11+}, and Mg^{8+}.

These simulations show that the contribution from the solar wind charge exchange process to the X-ray emissions from the halo is large enough to explain the observed X-ray flux [3].

Recent observations of X-rays from Mars using XMM-Newton [4] have provided new data that will enable us to refine the simulation models and increase our understanding of the physical processes involved.

---

* Electronic address: herbert.gunell@physics.org; URL: http://www.irf.se/~herbert
† Currently at NASA Goddard Space Flight Center, Laboratory for Solar and Space Physics, Mail Code 612.2, Greenbelt, MD 20771, USA

[1] K. Dennerl, "Discovery of X-rays from Mars with Chandra," *Astronomy & Astrophysics*, vol. 394, pp. 1119–1128, doi:10.1051/0004-6361:20021116, 2002.

[2] H. Gunell, M. Holmström, E. Kallio, P. Janhunen, and K. Dennerl, "Simulations of X-rays from solar wind charge exchange at Mars: Parameter dependence," *Adv. Space Res.*, in press, 2005.

[3] H. Gunell, M. Holmström, E. Kallio, P. Janhunen, and K. Dennerl, "X-rays from solar wind charge exchange at Mars: A comparison of simulations and observations," *Geophys. Res. Lett.*, vol. 31, L22801, doi:10.1029/2004GL020953, 2004.

[4] K. Dennerl, C. M. Lisse, A. Bhardwaj, V. Burwitz, J. Englhauser, H. Gunell, M. Holmström, F. Jansen, V. Kharchenko, and P. M. Rodríguez-Pascual, "Mars observed with XMM-Newton high resolution X-ray spectroscopy with RGS," submitted to *Astronomy & Astrophysics*, 2005.

Solar Wind Charge Exchange (SWCX)

Heavy, multiply charged, ions in the solar wind undergo charge exchange collisions with neutrals in the exosphere. For example:

$$O^{7+} + H \rightarrow O^{6+*} + H^{+}$$

This leaves an excited ion that returns to the ground state by emitting photons in the soft X-ray range.

$$O^{6+*} \rightarrow O^{6+} + h\nu$$

This process is responsible for the emission of X-rays from comets.

Simulation of charge exchange X-rays at Mars

1. The solar wind parameters are estimated from WIND data.
2. A 3D hybrid simulation using these input parameters $\Rightarrow \vec{E}$ and $\vec{B}$.
3. A test particle simulation for the heavy, multiply charged, ions (O^{7+}, C^{6+}, O^{6+}, O^{8+}, Mg^{10+}, Mg^{9+}, Si^{9+}, N^{6+}, C^{5+}, Ne^{8+}, Fe^{9+}, S^{9+}, Si^{8+}, Fe^{11+}, and Mg^{8+}).

Simulation technique

Hybrid and test particle simulations

Parameter estimation from WIND data

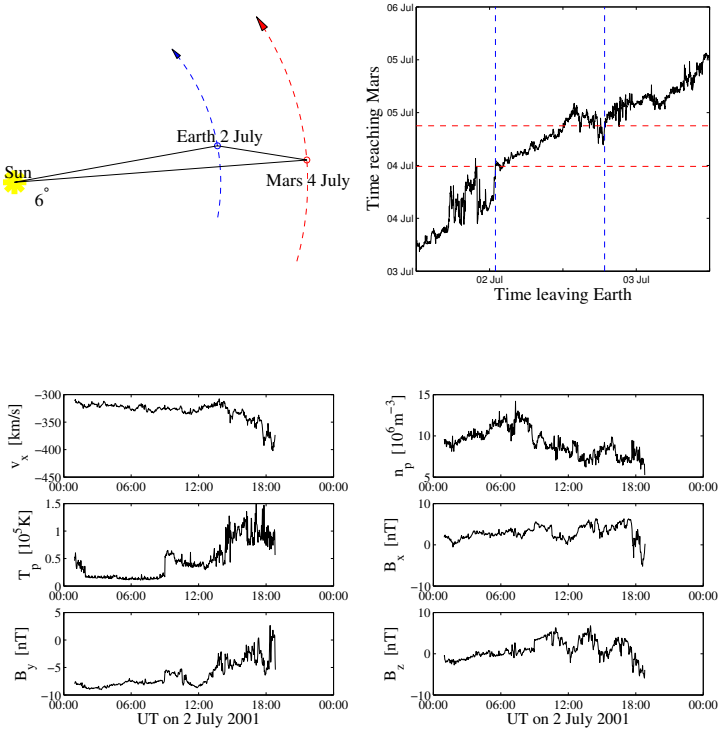

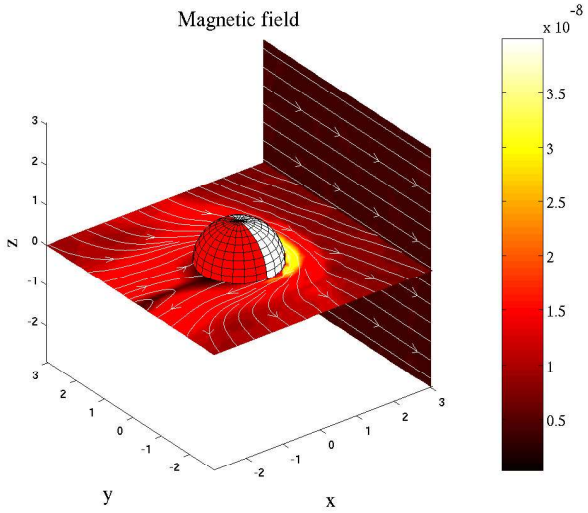

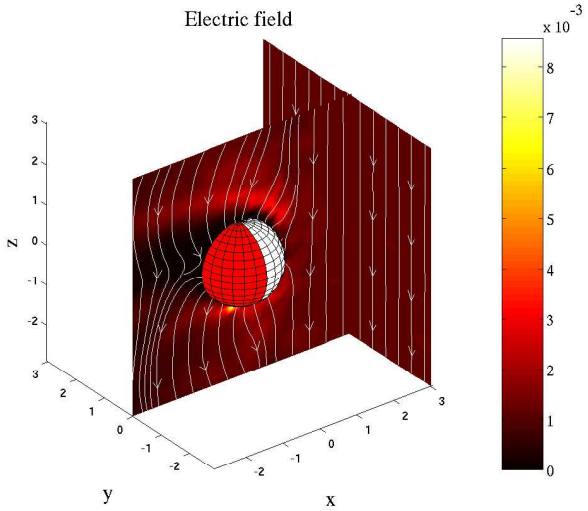

Average solar wind parameters at Mars on July 4, 2001, 11:47–21:00 (UT) as estimated from WIND data.

v_{sw}	330 km/s
n_{sw}	4.40×10^6 m^{-3}
$T_{p,sw}$	4.56×10^4 K
$\vec{B}$	$(1.13, -3.63, 0)$ nT =
	3.80 nT $\cdot (\cos(72.7°), -\sin(72.7°), 0)$

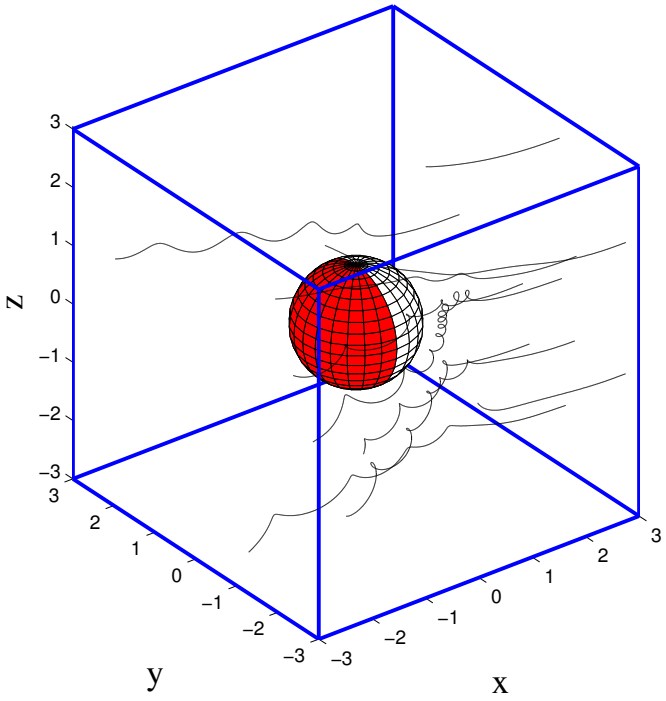

Comparison with observations

X-ray images

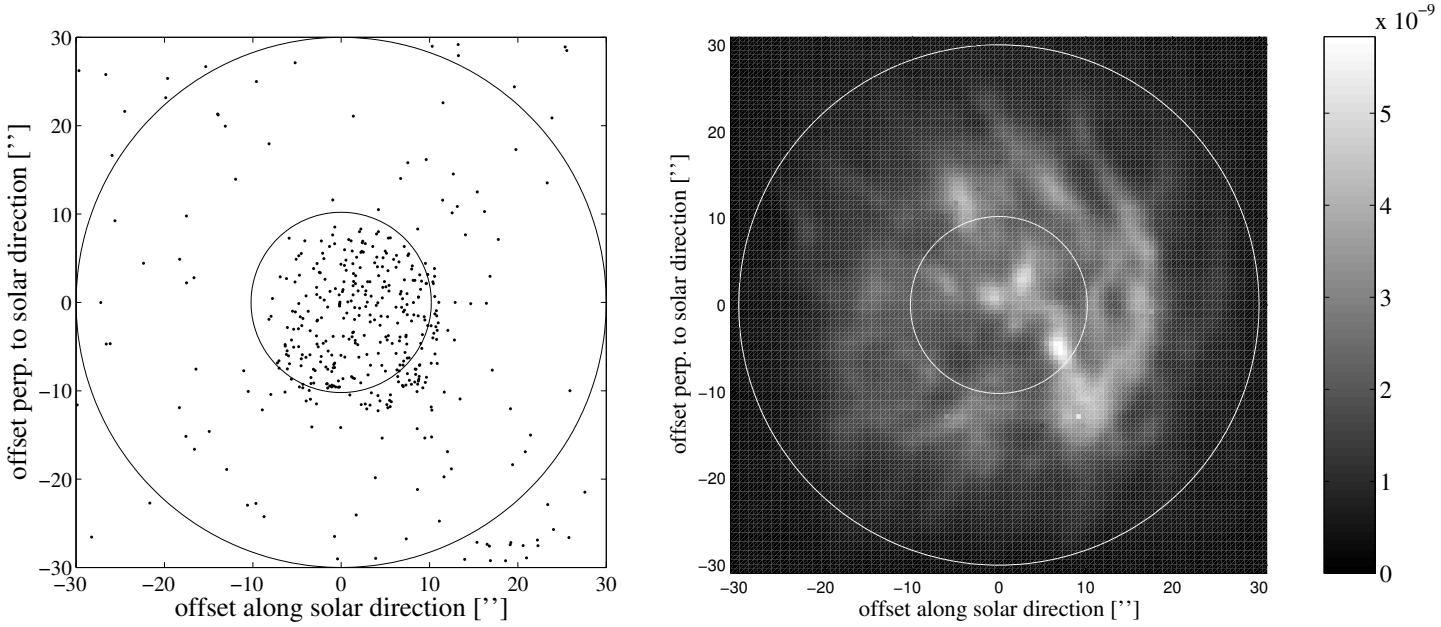

Left: X-ray photons with 0.2 keV$\leq E \leq$ 1.5 keV, observed on 4 July 2001. Right: A simulated X-ray image of Mars at a phase angle of 18.2°, corresponding to the situation at the time of the observation. The inner white circle, with radius 10.2 arc seconds, marks the geometric size of Mars, and the outer white circle, with radius 30 arc seconds marks the extent of the X-ray halo. The grey-scale shows the X-ray radiance in $\mathrm{Wm^{-2}sr^{-1}}$.

Radial distribution

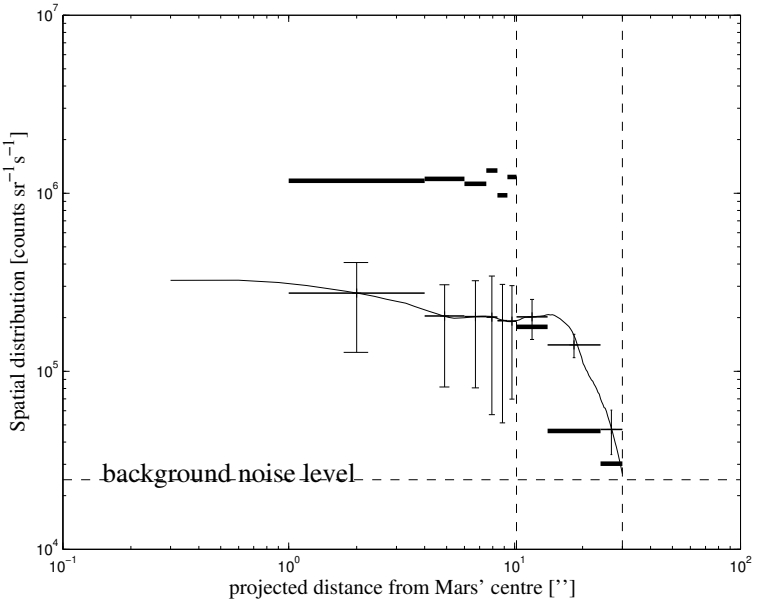

Radial distribution of the observed X-ray intensity in units of $\mathrm{sr^{-1}}s^{-1}$. The thin solid curve shows the results of the simulation. The horizontal thick lines are a histogram of the observed X-ray photons. The horizontal thin lines show the average X-ray intensity in the same intervals as the histogram of the observation. The error bars mark a 90% confidence interval of the simulated results, assuming a Poisson distribution for the count rate.

Parameter dependence 1

Average solar wind parameters at Mars on July 4, 2001, 11:47–21:00 (UT) as estimated from WIND data (left column), and through MHD tomography of interplanetary scintillation (IPS) data (right column).

	WIND	IPS
v_{sw}	330 km/s	434 km/s
n_{sw}	4.40×10^6 m^{-3}	2.63×10^6 m^{-3}
$T_{p,sw}$	4.56×10^4 K	5.61×10^4 K
$\vec{B}$	$(1.38, -4.43, 0)$ nT =	$(0.639, -0.915, 9.63 \times 10^{-4})$ nT =
	4.64 nT $\cdot (\cos(72.7°), -\sin(72.7°), 0)$	1.12 nT $\cdot (\cos(55°), -\sin(55°), 0)$

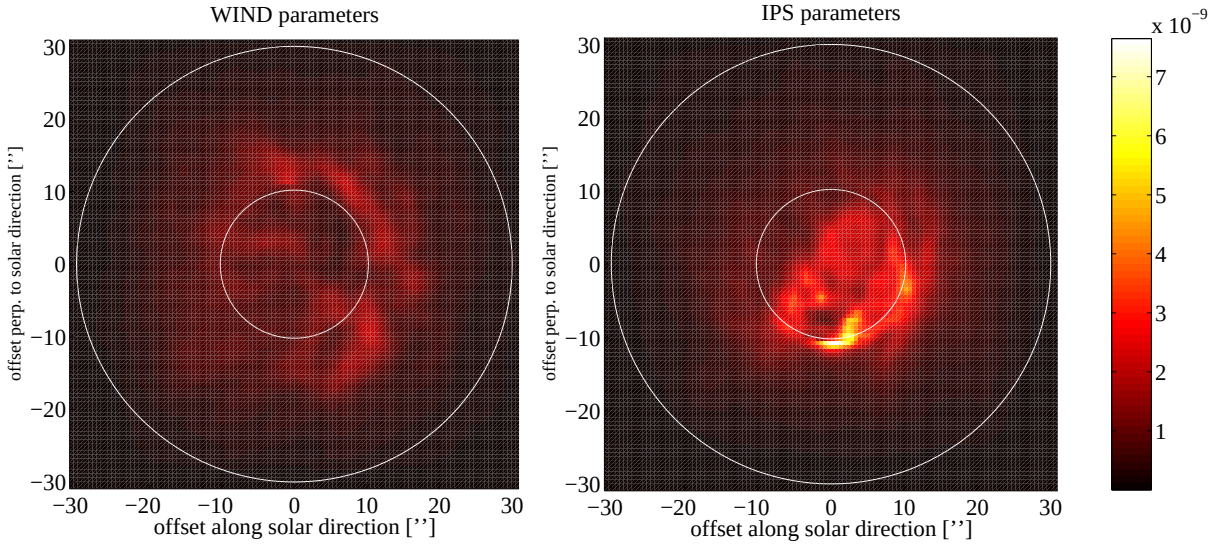

Two simulated X-ray images of Mars at a phase angle of 18.2°, corresponding to the situation at the time of the observation. The phase angle is defined as the angle between the Mars-to-sun and the Mars-to-observer directions. The left panel shows the results of a simulation with input parameters estimated from data obtained by the WIND satellite using a ballistic model. The right panel shows the results of a simulation with input parameters estimated using MHD tomography based on IPS measurements. The same colour-scale is used for both images, and it shows the X-ray radiance in Wm^{-2}sr^{-1}.

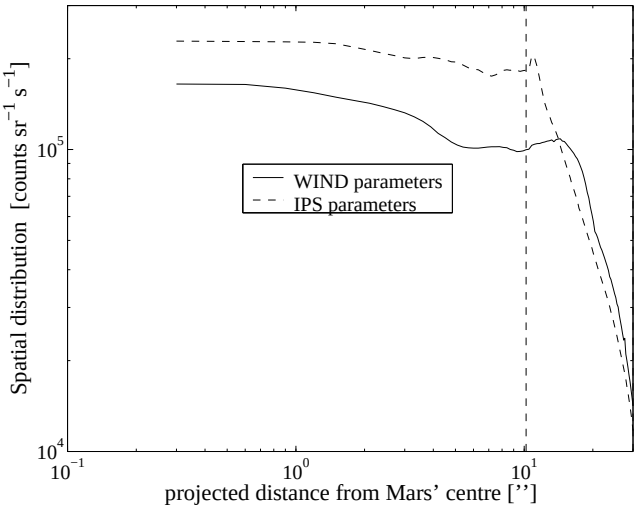

Radial distribution of the simulated X-ray intensity. The solid curve shows the results of a simulation using input data estimated from WIND data, and the dashed curve shows the results of a simulation with input data obtained by MHD tomography of IPS measurements. The vertical dashed line marks the size of the Martian disk, which corresponds to the inner circles of the images above.

Parameter dependence 2

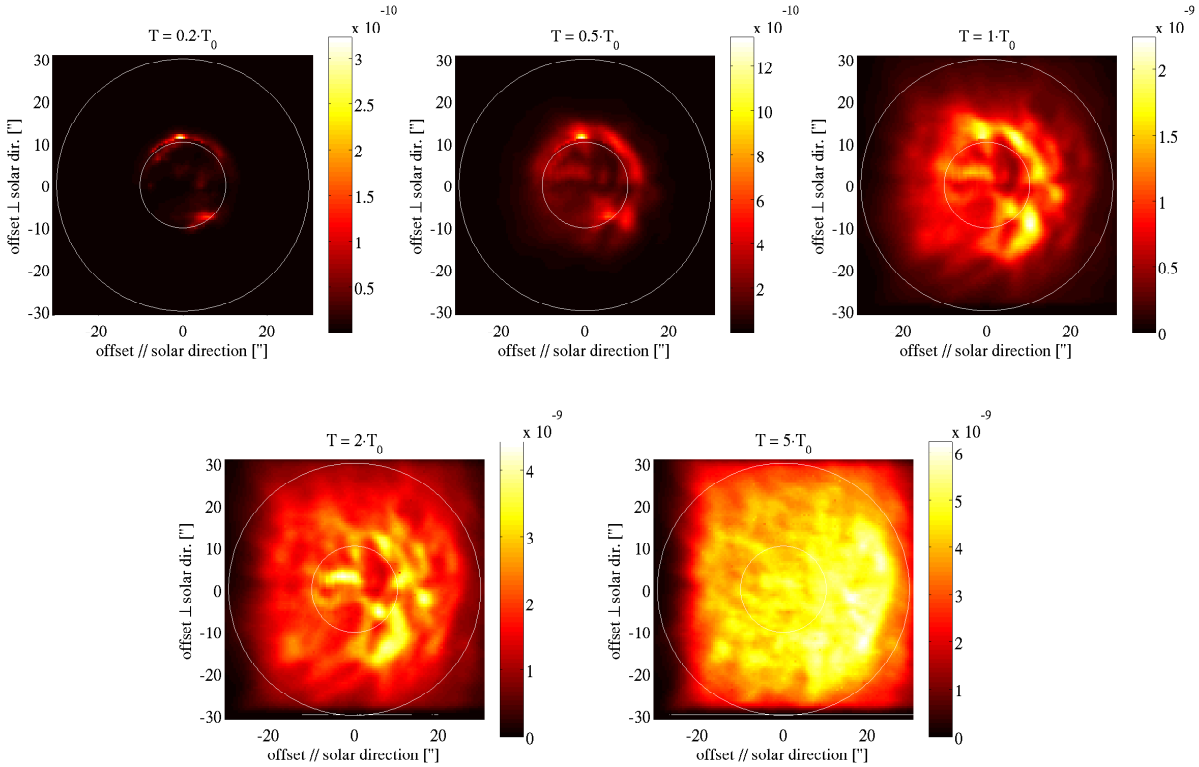

Five simulated X-ray image of Mars at a phase angle of 18.2°, corresponding to the situation at the time of the observation. The phase angle is defined as the angle between the Mars-to-sun and the Mars-to-observer directions. The different panels show results obtained assuming different exobase temperatures. From top to bottom the nominal exobase temperatures have been scaled by a factor of 0.2; 0.5; 1; 2; and 5 respectively.

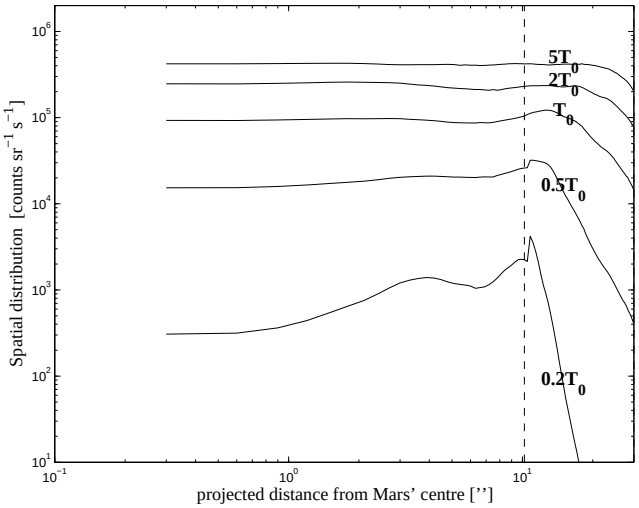

Radial distribution of the simulated X-ray intensity. The different curves show results obtained assuming different exobase temperatures. From top to bottom the nominal exobase temperatures have been scaled by a factor of 5; 2; 1; 0.5; and 0.2 respectively. The vertical dashed line marks the size of the Martian disk, which corresponds to the inner circles of the images above.

Nominal exobase densities and temperatures for the neutral species that are included in the exosphere model:

Species	H	H_2	$O_{thermal}$	O_{hot}
Density	3.1×10^{10} m^{-3}	4.3×10^{11} m^{-3}	3.3×10^{14} m^{-3}	3.1×10^{10} m^{-3}
Temperature	0.31 kK	0.37 kK	0.38 kK	4.6 kK

Mars observed with XMM-Newton 1

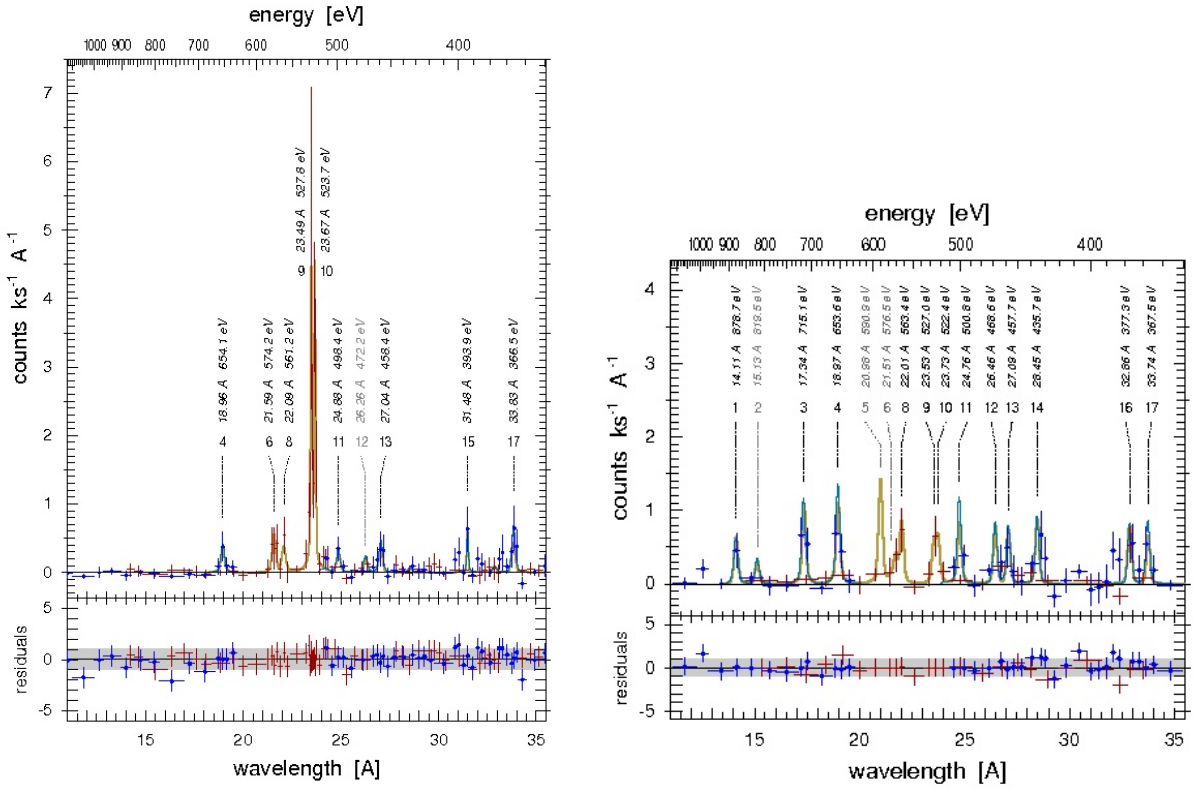

Mars was observed with the Reflection Grating Spectrometer (RGS) of XMM-Newton on 20–21 November 2003 [4]. The left panel shows a X-ray spectrum of the Martian disk and the right panel shows a spectrum of the halo.

line #	line abbr	wavelength [nm]	energy [eV]	ion	transition
1	Ne72	1.421	872.5	Ne^{7+}	$2p \rightarrow 1s$
2	O74	1.518	817.0	O^{7+}	$4p \rightarrow 1s$
3	O65	1.740	712.5	O^{6+}	$5p \rightarrow 1s$
4	O72	1.897	653.6	O^{7+}	$2p \rightarrow 1s$
5	N63	2.091	593.0	N^{6+}	$3p \rightarrow 1s$
6	O6r	2.161	574.0	O^{6+}	$2^1P_1 \rightarrow 1^1S_0$
7	O6i	2.181	568.5	O^{6+}	$2^3P_1 \rightarrow 1^1S_0$
8	O6f	2.211	560.9	O^{6+}	$2^3S_1 \rightarrow 1^1S_0$
9	CO2a	2.350	527.7	CO_2	$1\pi_g \rightarrow 1s$
10	CO2b	2.368	523.5	CO_2	$3\sigma_u^{(\star)} \rightarrow 1s$
11	N62	2.478	500.3	N^{6+}	$2p \rightarrow 1s$
12	C55	2.636	470.4	C^{5+}	$5p \rightarrow 1s$
13	C54	2.699	459.4	C^{5+}	$4p \rightarrow 1s$
14	C53	2.847	435.6	C^{5+}	$3p \rightarrow 1s$
15	N22	3.147	394.0	N_2	$3\sigma_g \rightarrow 1s$
16	C45	3.275	378.5	C^{4+}	$5p \rightarrow 1s$
17	C52	3.374	367.6	C^{5+}	$2p \rightarrow 1s$

* Also the transitions $4\sigma_g \rightarrow 1s$ and $1\pi_u \rightarrow 1s$ may contribute to this line.

Individual lines can be identified in the spectra. This will enable us to improve the computer models, and to study the behaviour of different ion species in more detail.

Mars observed with XMM-Newton 2

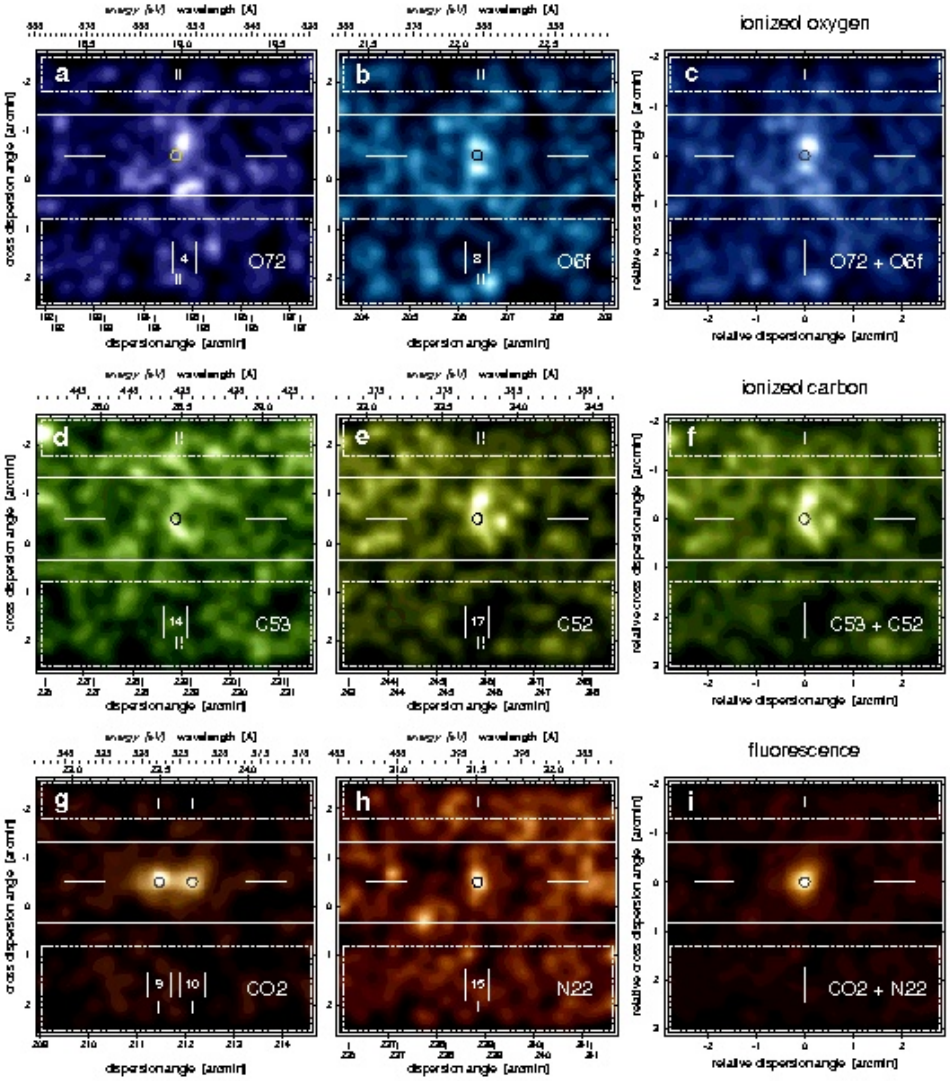

RGS images of Mars and its halo in the individual emission lines of ionised oxygen (top row), ionised carbon (middle row), and fluorescence of CO_2 and N_2 molecules (bottom row).

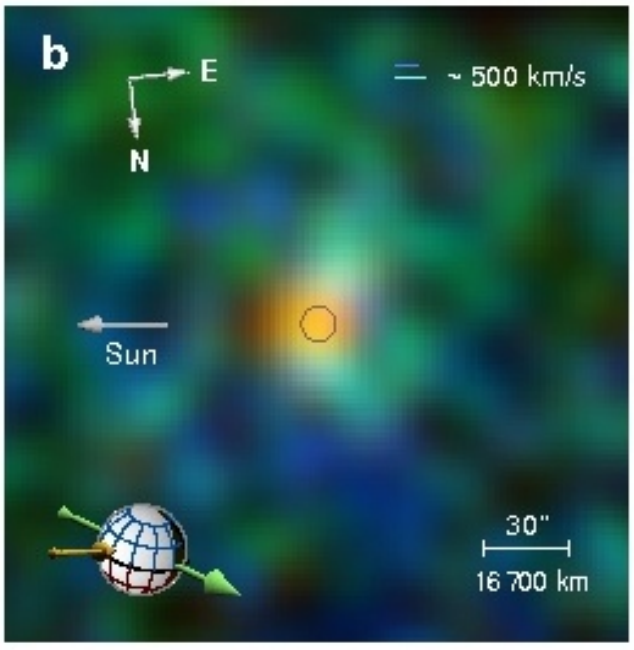

Superposition of the images in the figure above, each centred on the wavelength/energy of an individual emission line, with ionised oxygen coded in blue, ionised carbon in green, and fluorescence coded in yellow and red.